Propagation mechanisms of radio waves over intra-chip channels with integrated antennas : frequency-domain measurements and time-domain analysis

Zhang, Yue Ping; Chen, Zhiming; Sun, Mei

2007

Zhang, Y. P., Chen, Z. M., & Sun, M. (2007). Propagation mechanisms of radio waves over intra-chip channels with integrated antennas: Frequency-domain measurements and time-domain analysis. IEEE Transactions on Antennas and Propagation, 55(10), 2900-2906.

https://hdl.handle.net/10356/91522

https://doi.org/10.1109/TAP.2007.905867

Propagation Mechanisms of Radio Waves Over Intra-Chip Channels With Integrated Antennas: Frequency-Domain Measurements and Time-Domain Analysis

Yue Ping Zhang, Zhi Ming Chen, *Student Member, IEEE*, and Mei Sun

***Abstract*—The propagation mechanisms of radio waves over intra-chip channels was studied with integrated antennas for wireless chip area networks. Test vehicles were designed and fabricated on silicon wafers of both low and high resistivities, respectively, using complementary metal oxide semiconductor (CMOS) processes. On-wafer measurements for propagation of radio waves over intra-chip channels were conducted in the frequency domain from 10 to 110 GHz with a network analyzer. Time-domain analysis was performed to characterize intra-chip radio channels and more importantly to understand the propagation mechanisms. It was found that path loss factor is constantly less than two and propagation delay of the first-arrival wave is significantly longer than that by free-space transmission. Thus, we concluded that the propagation of radio waves over intra-chip channels is mainly realized with surface wave rather than space wave. Surface wave is guided on air-wafer interface. In addition, effects of metal lines, in both parallel and normal placements with respect to wave propagation direction, on signal propagation were also investigated.**

***Index Terms*—Channel modeling, intra-chip, wireless chip-area network, wireless interconnect.**

I. Introduction

CMOS technology has been continuously scaling down in order to improve device performance. Recently, MOS transistor feature dimension has been scaled below 100 nm and the speed of operation has exceeded over 100 GHz. CMOS technology scaling causes great interconnect challenges. On one hand, the width and thickness of metal interconnect lines are scaled down in proportion with device feature dimension. On the other hand, metal wires have to be routed over a bigger chip area for ultra-large scale integration (ULSI) or system-on-chip (SoC) solutions. As a result, the fundamental material limit of wire interconnect will be approached sooner or later. In other words, traditional wire-interconnect has become a bottleneck in further development of ULSI or SoC. To carry on the progress of current and future ULSI or SoC, wireless interconnect has been proposed. Floyd *et al.* have developed on-chip antennas, which were integrated with transmitter and receiver, for wireless clock distribution [1]. Zhang has evaluated intra-chip data communication using wireless interconnect [2]. More recently, the idea of wireless interconnect has been extended to the concept of wireless chip area networks. A wireless chip area network uses radio waves rather than metal wires to communicate among cores within a chip (intra-chip) or among chips within a module (inter-chip) [3]–[6].

The wireless chip area network features a unique intra/inter chip-scale radio propagation channel. It is known that understanding of chip-scale radio propagation channels is essential for the analysis and design of a wireless chip area network. Chen and Zhang have studied an inter-chip radio propagation channel with on-package monopoles over the ultra wideband frequency range from 3.1 to 10.6 GHz [7]. As expected, the inter-chip radio propagation channel is a multi-path radio propagation channel and the received radio signal suffers from frequency-selective fading and time-domain dispersion. The propagation loss depends on whether the inter-chip radio propagation channel is located in an open or enclosed casing. The path loss factor is less than 2 in the enclosed casing and larger than 2 in the open casing. Kim *et al.* have studied an intra-chip propagation channel in the frequency domain from 6 to 18 GHz with integrated dipoles on a silicon wafer [8]. They proposed a plane-wave model to explain the propagation mechanisms and found transmission gain can be improved by inserting a low-loss dielectric layer between the silicon wafer and the probe-station chunk, which functions as a ground plane.

Integrated or on-chip antennas excite and receive radio signal in an intra-chip propagation channel. Being inseparable from the intra-chip propagation channel, an on-chip transmitting antenna, an intra-chip propagation channel, and an on-chip receiving antenna are considered in this paper as an intra-chip radio propagation channel. The intra-chip radio propagation channel has been characterized on transmission gain [9]–[12]. Kim and O measured the transmission gain in the frequency domain from 10 to 18 GHz for axially 2-mm long straight dipoles fabricated on bulk, silicon-on-insulator (SOI) and silicon-on-sapphire (SOS) substrates [9]. They found that the transmission gain of dipoles increases with frequency and has higher value on the SOS substrate than those on the bulk and SOI substrates. The lower transmission gain for dipoles on the bulk and SOI substrates is due to the low resistivity of the substrates, which has a higher loss as compared to the SOS substrate. Resistivity of silicon substrate can be greatly

Manuscript received November 7, 2006; revised February 14, 2007.

The authors are with the School of Electrical and Electronic Engineering, Nanyang Technological University, Singapore 639798, Singapore (e-mail: eypzhang@ntu.edu.sg; chen0185@ntu.edu.sg; SunMei@ntu.edu.sg).

Digital Object Identifier 10.1109/TAP.2007.905867

increased by proton implantation, leading to a lower substrate loss and therefore a higher transmission gain [11]. A high transmission gain window in frequency domain was observed from measurements of on-chip monopoles up to 110 GHz [12]. The wireless chip area network is recommended to operate within the high-gain window for optimized performance. In addition, there are many metal structures such as bus lines, power lines, and solder joints, which inevitably occur between transmitting and receiving antennas and affect the characteristics of the intra-chip radio propagation channel. It was found that the parallel and normal metal lines between antenna pair increase and decrease the transmission gain, respectively [10].

Literature survey shows that the intra-chip radio propagation channel has been measured and analyzed in frequency domain. Yet, no time-domain analysis of intra-chip radio propagation channel has been made. As a result, available received power and delay-spread characteristics of the intra-chip radio propagation channel are still not clear. The intra-chip radio propagation channel has not been fully characterized, which necessitates the work performed in this paper. We describe the test vehicles, integrated antennas, and frequency-domain measurements in Section II. We analyze characteristics of intra-chip radio propagation channel in time-domain and offer a physical insight into propagation mechanism in Section III. Finally, we summarize the findings in Section IV.

II. Frequency-Domain Measurements

Integrated monopoles, test vehicles, measurement setup, and frequency-domain results are described in this section.

A. Integrated Monopoles and Test Vehicles

Dipole antennas are preferred for wireless chip area networks because they can adequately reject noise and interfering signals generated by other circuits on the same substrate. However, dipole antennas are not compatible with most currently existing test facilities. Baluns are required to have the measurement done for dipoles. It is known that baluns are narrowband devices, which partially explains why most reported frequency-domain measurements are below 26.5 GHz [12]. To experimentally characterize intra-chip radio propagation channels over a much broader bandwidth, integrated monopole antennas, including zigzag, linear, and meander antennas, were laid out on standard 6-in p-type silicon wafer, whose cross-sectional view is depicted in Fig. 1. An oxide layer of thickness 2 μm is grown on silicon substrate of thickness 633 μm for isolation. Monopole antennas with axial length 1 mm are drawn using aluminum layer of 2 μm thickness and 10 μm width. Monopoles were then fabricated into test vehicles using NTU 1.2-μm CMOS process, where resistivity of silicon wafers are 10 $\Omega-$ cm and 5 k$\Omega-$cm, respectively. The maximum size of a test vehicle is 10.8×10.8 cm^2 [12].

Antennas, once integrated on a substrate, are impossible to move or rotate with respect to each other. Therefore, in order to cover various scenarios for the characterization of intra-chip radio propagation channels, monopole antenna pairs separated at a specific distance d between the transmitting and receiving (T-R) antennas and oriented with a specific angle were designed as shown in Fig. 1. Sixteen pairs of monopole antennas with a

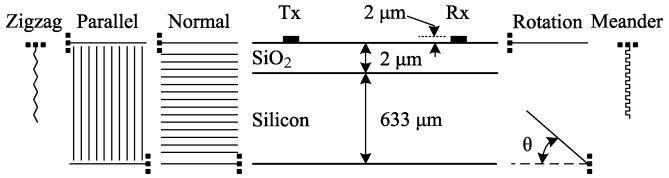

Fig. 1. Cross-sectional and top views (not to scale) for integrated zigzag, linear and meander antennas on silicon wafer.

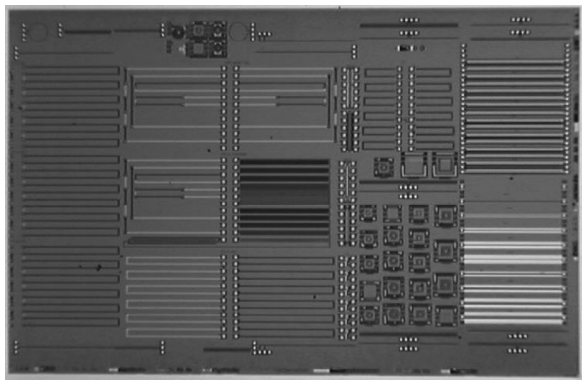

Fig. 2. Die photo of a test vehicle using 0.18 μm process.

2.5-mm increment in T-R distance and 10 pairs of monopole antennas with a 10° increment in relative angle were implemented in test vehicles, which cover separation from 2.5 to 40 mm and relative angle from 0° to 90°. As shown in Fig. 1, metal lines, which can be densely or loosely spaced, were placed between monopole antenna pairs in both parallel and normal directions. By parallel and normal directions, we mean metal lines are placed parallel and normal to wave propagation direction, respectively.

In addition, another test vehicle was designed and fabricated together with other circuits on a standard 8-in p-type silicon wafer of low resistivity 10 $\Omega-$ cm using the state of the art 0.18-μm CMOS technology. An oxide layer of thickness 26 μm was grown on silicon substrate of thickness 750 μm for isolation [13]. Monopole antennas with axial lengths of 1 and 2 mm were implemented using copper layer of 4 μm thickness and 30 μm width. A die photo for the test vehicle using 0.18 μm process is shown in Fig. 2, where there are dipoles, inverted-F, and loop antennas with complex circuits placed in between.

B. Measurement Setup and Frequency-Domain Results

The measurement setup consists of a MicroTech probe station and an HP8510XF network analyzer to get the S-parameters in the frequency range of 10–110 GHz, as depicted in Fig. 3. It is seen that the test vehicle wafer is mounted on the metal chunk of the probe station. Having calibrated the network analyzer with the standard cal kit and procedures, we conducted the reflection measurements to obtain S11 and S22 and the transmission measurements to obtain S12 and S21. The results of reflection measurements at various distances d are displayed in Fig. 4 for meander monopoles on both high- and low-resistivity silicon wafers. It is evident that S11 is insensitive to the T-R separation distance. Over the whole frequency range, there is no sharp resonance dip observed for antennas on the 10 $\Omega-$ cm silicon

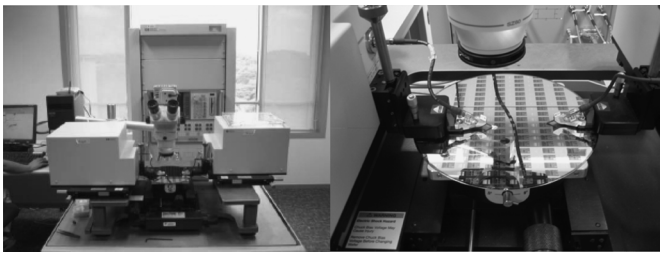

Fig. 3. Setup for frequency domain measurement of on-chip monopoles.

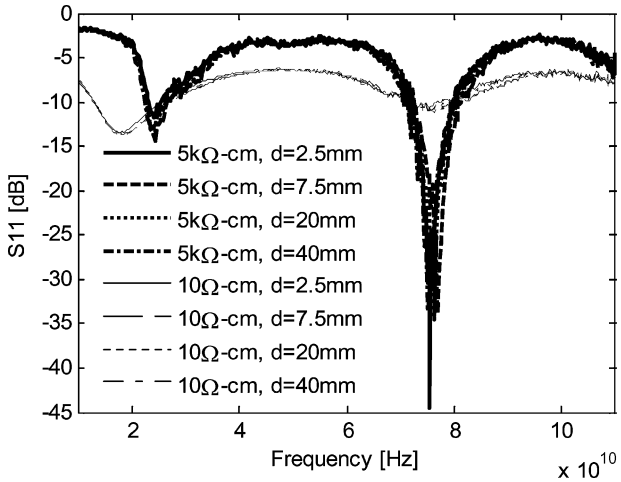

Fig. 4. Measured S11 versus frequency for meander antennas.

wafer. In contrast, sharp resonance dips can be seen at 25 and 75 GHz for meander monopoles on the 5 $\mathrm{k}\Omega - \mathrm{cm}$ silicon wafer. The matching of monopole antennas on the 5 $\mathrm{k}\Omega - \mathrm{cm}$ silicon wafer over the whole frequency range from 10 to 110 GHz is not good for applications in a real system but is acceptable for the application in the channel characterization. This is because the matching affects the transmitted and received power, so does the performance of the real system, however, the matching will not affect the path loss factor, delay spread and the propagation mechanisms.

As examples, the transmission coefficient S21 are shown in Fig. 5 for the zigzag monopole antenna pairs on both high- and low-resistivity silicon wafers at the T-R separation of $d = 5\ \mathrm{mm}$. The high S21 windows can be seen in the frequency range from 15 to 30 GHz and 25 to 60 GHz for the low and high-resistivity silicon wafers, respectively. Within the high S21 windows, phase responses are linear or nearly linear indicating clearly that the radio signal transmission between the monopole antennas occurs through the propagation of a dominant mode or path [12].

Fig. 6 shows the effects of metal interference structures on the transmission between a pair of linear monopole antennas on high-resistivity substrate. It is observed that the existence of metal lines improves gain within the S21 window. This is because the periodic layout of the metal lines enhances the band pass characteristic of the intra-chip radio propagation channel [12]. This characteristic can be used wisely to improve antenna transmission gain performance.

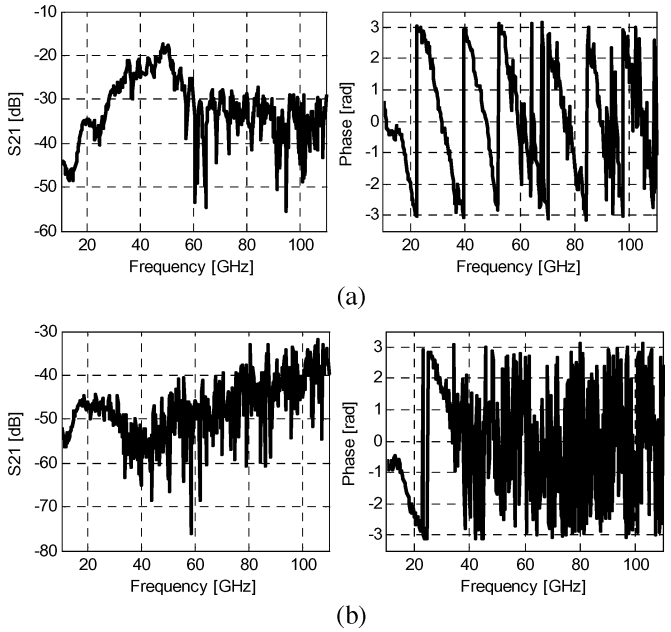

Fig. 5. Magnitude and phase responses of S21 for the zigzag antenna pairs at $d = 5\ \mathrm{mm}$. (a) High resistivity substrate; (b) low resistivity substrate.

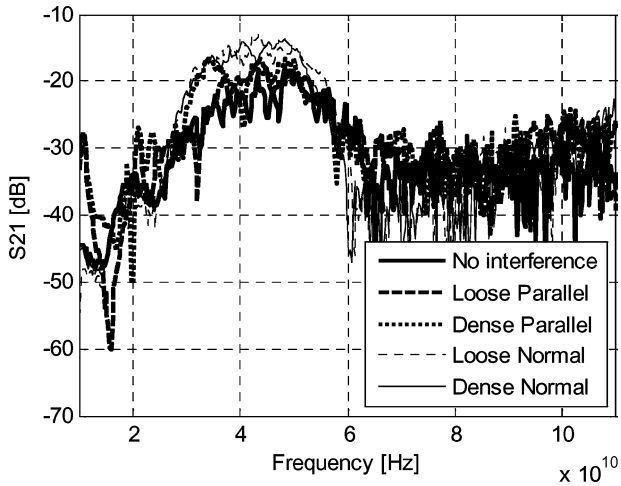

Fig. 6. Effect of metal interference structures on the magnitude of S21 of linear antenna pairs at $d = 5\ \mathrm{mm}$.

Fig. 7 compares the magnitudes of the transmission coefficient S21 measured for zigzag antennas at the T-R separation of $d = 10\ \mathrm{mm}$ on the 10 $\Omega - \mathrm{cm}$ silicon wafers fabricated using both 1.2-μm and 0.18-μm CMOS processes. It is seen that the transmission is significantly improved over the frequency range from 20 to 40 GHz, by the 26 μm thick oxide layer and better conducting material, which is copper.

III. Time-Domain Analysis

Based on observation of reflection and transmission coefficients, frequency range, which favors signal transmission, can be determined. However, information provided by analysis in frequency domain only is not sufficient for the design of wireless chip area networks. Total power attenuation and delay spread of channel impulse response (CIR) determines transmitter/receiver

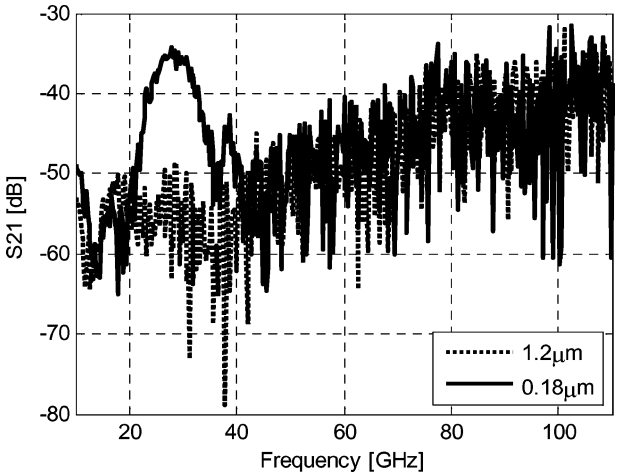

Fig. 7. Magnitude responses of S21 for zigzag antennas at $d = 10\,\mathrm{mm}$.

gain and number of taps to capture enough energy for demodulation. Furthermore, the upper limit of data rate is set by the channel time-domain characteristics as well.

Characterization of intra-chip channel in time domain requires a fine resolution to differentiate rays from different paths. Direct measurement could be difficult in designing extremely narrow transmitted pulse and obtaining high time domain resolution. Due to the Fourier transform relationship between time domain and frequency domain signals, measurement in frequency domain is a good alternative for short-range time domain channel characterization, which requires fine resolution. CIR can be converted from transmission coefficient S21 using inverse discrete Fourier transform (IDFT). The obtained CIR has a corresponding time domain resolution $1/2B$, where B is the measurement frequency span [7]. A high value of B is necessary for a fine time domain resolution, making rays from different paths differentiable. Further more, measurement range has to cover the high-gain window, which spreads over 13 to 65 GHz for antennas on high-resistivity substrate [12].

Through observation over the received power delay profile, resistivity of silicon wafer significantly affects the received signal power. As a comparison, received power delay profiles of zigzag antennas at the T-R separation of $d = 5\,\mathrm{mm}$ are shown in Fig. 8 for both low and high resistivity silicon wafers. It can be seen that received power delay profile peak for the antenna pair on the low-resistivity silicon wafer has been heavily attenuated by more than two orders of magnitude, as compared to that for antennas on high-resistivity silicon wafer. Besides, the received power delay profile peak for the low-resistivity case is only a few times above the noise floor at 5 mm. The noise floor is set to 10 dB above average noise. Noise floor for the low-resistivity substrate is $6.4 \times 10^{-7}\ \mathrm{V}^2$, as plotted in Fig. 8. However, for the high resistivity substrate, noise floor of $8.6 \times 10^{-7}\ \mathrm{V}^2$ cannot be observed as it is around 3 orders of magnitude lower than the signal peak. Further increasing the T-R separation to $d = 10\,\mathrm{mm}$ gives a received power delay profile, which is entirely buried in noise. Generally, there is more than 10 dB extra power loss for monopoles integrated on the low-resistivity silicon wafer than those on the high-resistivity silicon wafer, and this difference can be up to 17 dB in

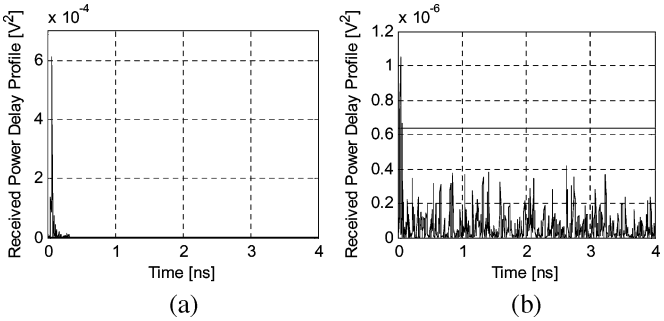

Fig. 8. Received power delay profile of the zigzag antenna pairs at $d = 5\,\mathrm{mm}$: (a) high resistivity substrate (b) low resistivity substrate.

extreme cases, making low-resistivity substrate an inferior candidate in on-chip antenna applications. Therefore, it is highly recommended that the proton implantation technique be used to increase the resistivity of silicon wafer [11], [14] for wireless intra-chip radio communications. The proton implantation technique has negligible degradation on gate oxide integrity [14]. The following analysis will focus on the intra-chip radio propagation channel on the high-resistivity silicon wafer since the low-resistivity silicon wafer leads to a much higher loss and the transmitting power and receiving sensitivity of our measurement setup is limited and the propagation mechanisms cannot be well revealed.

By inspection over all the power delay profiles obtained, energy decays completely within 1 ns. To reduce the effect of noise on analysis results, noise component needs to be removed. Therefore, the time segment from 1 to 2 ns is selected to determine the average noise floor. Bins in a power delay profile below certain threshold are considered as no energy, where the threshold is set to be 10 dB above the average noise floor.

A. Path Loss

To understand the relationship between power attenuation and T-R separation, power loss in dB is plotted over log distance and fitted using

$$PL = \gamma 10 \log_{10}(d/d_0) + PL_0 + X_\sigma \tag{1}$$

where γ, d_0, PL_0 are the path loss (PL) factor, reference distance and intercepted PL at d_0 respectively. X_σ is a zero-mean Gaussian-distributed random variable in dB with standard deviation σ to cover the shadowing effect [15]. The scatter plot and fitted lines for zigzag, meander and linear antennas are shown in Fig. 9. The respective parameters of (1) are summarized in Table I for the three antennas.

Good fitting qualities of PL can be observed as the standard deviations of the random variable X_σ are quite small. Another interesting observation is that the PL factor γ is significantly lower than the free-space PL factor, which is equal to 2. It implies that signal is not carried through space wave. Instead, the wave propagation is through some manner of guided wave.

Metal interference structures, either in parallel or normal placement, improve transmission as compared to the T-R pairs without metal structures in between. This is because the periodic layout of metal lines enhances the bandpass characteristics

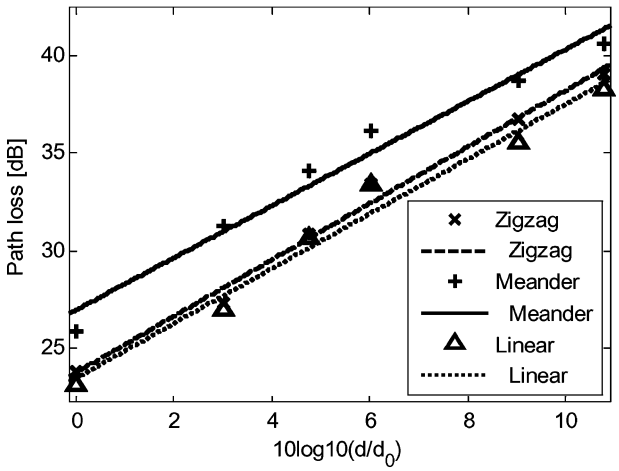

Fig. 9. PL versus log distance for zigzag, meander and linear monopole antennas.

TABLE I
PL PARAMETERS FOR ANTENNAS

	γ	PL_0 (dB)	σ (dB)
Zigzag	1.454	23.7	0.5587
Meander	1.342	26.93	0.8736
Linear	1.411	24.41	0.8276

TABLE II
EFFECTS OF INTERFERENCE STRUCTURES ON PL FOR ANTENNAS

	Zigzag	Meander	Linear
No interference	27.322	31.245	26.97
Loose parallel	26.809	28.071	25.501
Dense parallel	25.099	25.872	24.3
Loose normal	22.367	24.6	21.769
Dense normal	24.985	24.453	21.92

of the intra-chip radio propagation channel. However, other interference structure, such as floating metal lines in both normal and parallel directions, reduces the transmission gain slightly. Metal plate placed between antenna pair degrades received signal further [10], [16]. On the other hand, discontinuous metal blocks of 10 μm $\times$ 10 μm do not reduce transmission gain seriously [16]. PL for antennas with different interference metal lines is compared with no interference situations in Table II. An important observation is that a normal interference structure gives an even lower PL than that by the parallel metal lines, which is opposite to observation made in [10]. However, there is no conflict between the two observations. In [10], the sampled frequency range is below 26.5 GHz. They could not find the high-gain window located roughly from 25 to 60 GHz, which is the dominant range that contributes to the received signal in our study, as shown in Fig. 6.

Relative angle between transmitting and receiving antennas changes the received signal strength as well. With respective to the relative rotation angle θ, variations of PL are summarized in Table III. As θ increases, due to polarization mismatch, PL gradually increases. The loss by antenna rotation can be up to 4 dB when linear antennas are placed normal to each other.

TABLE III
EFFECT OF ROTATION ON PL IN dB

θ (degrees)	Zigzag	Meander	Linear
0	28.032	31.142	27.517
30	28.423	31.238	27.226
45	28.784	32.538	28.164
60	30.137	33.391	29.687
90	30.974	33.994	31.624

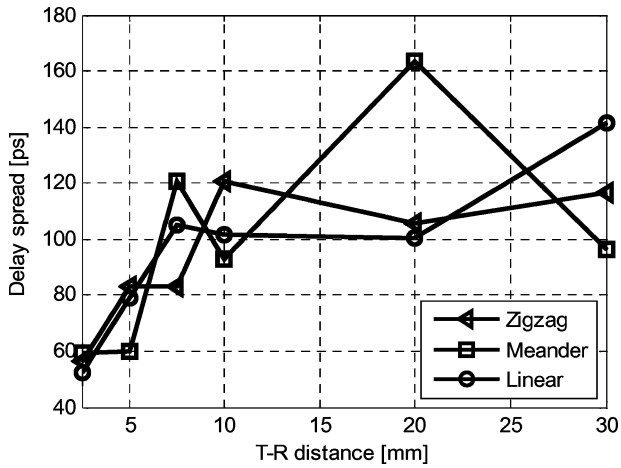

Fig. 10. Delay spread versus the separation distance between the transmitting and receiving antennas.

B. Delay Spread

Apart from total power attenuation, delay spread is another important factor for a radio propagation channel. As a measure of effective length of a CIR, delay spread covers major portion of the received signal energy. For different antennas, delay spread is plotted over the T-R separation distance in Fig. 10. It can be observed that delay spread generally increases with the T-R separation, although delay spread for a specific CIR depends on the surrounding of the T-R pair. In other words, receiver signal energy spreads over a longer time span with increased T-R separation distance.

When interference structures are placed between antenna pairs, it is found that metal lines, either in parallel or normal placement, help reduce delay spread for both zigzag and linear antennas. Another interesting observation is that for all antennas, with parallel interference structures, densely placed metal lines give a lower delay spread than that for loosely placed metal lines. However, for normal interference structures, dense metal lines lead to a higher delay spread than loose metal lines. It is due to the fact that parallel interference structures help guide the wave propagation, while normal metal lines tend to scatter the energy away [10].

C. Propagation Mechanisms

In addition to the characterization of intra-chip radio propagation channels, the understanding of the propagation mechanisms is very important for intra-chip radio communications. With the knowledge of the propagation mechanisms over the intra-chip radio channels, we can design more efficient integrated antennas, minimize electromagnetic interference, etc.

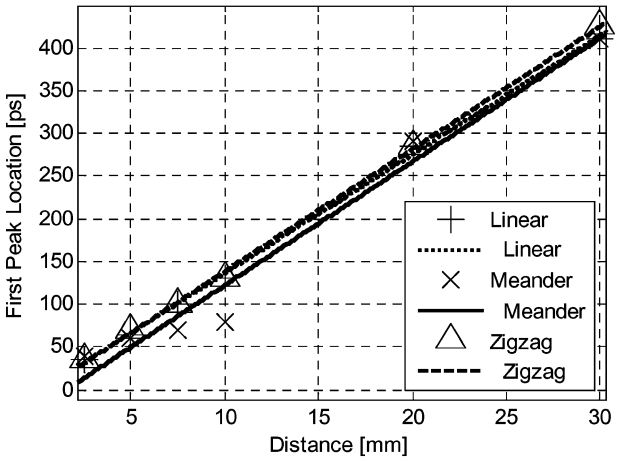

Fig. 11. Scatter and fitted lines for first arrival locations over distance.

To understand the propagation mechanisms, the first arrival for each CIR is located. It is found that the first peak arrives significantly later than the propagation delay calculated from the space wave, implying again that propagation is through some manner of guided waves. Antennas pairs with parallel interference structure give shorter delay than antennas without interference. In contrast, normal metal lines result in longer delay than the no-interference situation. For antenna pairs without interference metal lines, the relationship between first peak location and distance is plotted over linear distance in Fig. 11. The scatter plot of first peak location has been fitted into linear equation and a good fitting quality can be observed, especially for linear and zigzag antennas. The good fitting indicates that the propagation mechanisms are the same for antennas placed at various separation distances.

Generally, there are three types of waves based on which signal can propagate: space wave through air, surface wave by the air-wafer interface, and guided wave within the wafer. Leaky wave is not considered here, because it leaks energy continually into the direction perpendicular to the wafer surface, decreases exponentially over the intra-chip radio channel, and thus contributes to the received signal negligibly in the far-field region. Space wave is supported as if there were no wafer but an infinite air space. Surface wave occurs near the interface between the air and wafer as if air and wafer extended infinitely into their respective sides. Guided wave is realized by the reflection within the wafer. As the T-R separation increases, surface wave constitutes the dominant contribution because of its cylindrical characteristics as opposed to the spherical behaviour of space wave [17] and also the large attenuation of guided wave due to lossy wafer. It is known from [18] that for an integrated antenna on a dielectric substrate of high permittivity there is more energy carried by surface wave than by space wave when the ratio d/λ_0 is greater than 0.045, where d and λ_0 are the substrate thickness and free-space wavelength respectively. With d/λ_0 increasing up to 0.15, surface wave becomes more dominant over space wave. As the high window is in the range of 25 to 60 GHz here, the corresponding d/λ_0 is between 0.053 and 0.127; surface wave dominates in the propagation over the intra-chip channel.

As mentioned above, PL factor is significantly less than 2; therefore, space wave is impossible to be the dominant contribution to received signal. First arrival is not transmitted by space wave, since it arrives much later than free space transmission. Furthermore, the linear relationship between first arrival location and T-R distance excludes the possibility that first arrival is received through a reflected wave. As a result, it can be summarized that space wave contributes negligibly to the received signal and surface wave is the dominant path of received signal. Integrated antennas for intra-chip radio communications should be designed to launch effectively the surface wave rather than space wave.

IV. Conclusion

Monopole antennas have been fabricated on both high and low resistivity substrates. Measurement of monopoles in frequency domain up to 110 GHz shows that antennas on high-resistivity substrate have a much higher transmission coefficient than those on low-resistivity one. However, with oxide layer of 26 μm rather than 2 μm, an improvement of 15 dB can be observed within the high gain window for low-resistivity substrates.

Time domain power delay profile has been obtained from frequency measurement with a fine time domain resolution 5 ps. With T-R distance greater than 7.5 mm, received signal is buried entirely in noise for antennas on low-resistivity substrate with 2 μm thick oxide layer. For different antennas on high resistivity substrate, good fittings of PL over logarithmic distance give PL factor constantly less than two. It is also observed than first arrival is significantly later than free-space propagation. Therefore, it is concluded that dominant contribution to received signal is through surface waves, instead of space waves. Delay spread generally increases with T-R separation, and does not exceed 165 ps for different antennas up to 30 mm.

Metal lines, placed parallel or normal to propagation direction, reduces PL, due to enhanced bandpass characteristics of intra-chip radio propagation channel. Besides, delay spread is reduced with interference structures. Further more, as added metal lines change the relative permittivity of propagation medium, propagation delay is shortened with respect to antenna pair without interference structures. Effects of metal line density on the above three parameters have been studies as well. In addition, PL increases as relative angle antenna pairs increases due to polarization mismatch.

With characterization of intra-chip radio channels in time domain, design guidelines can be derived for intra-chip radio transceivers. System architecture, required gain, number of taps etc can be determined from channel parameters for optimized performance. Inevitable metal lines placed between antenna pairs can be designed in the way which favors signal transmission as well.

References

[1] B. A. Floyd, C.-M. Hung, and K. K. O, "Intra-chip wireless interconnect for clock distribution implemented with integrated antennas, receivers, and transmitters," *IEEE J. Solid-State Circuits*, vol. 37, no. 5, pp. 534–552, May 2002.

[2] Y. P. Zhang, "Bit-error-rate performance of intra-chip wireless interconnect systems," *IEEE Commun. Lett.*, vol. 8, no. 1, pp. 39–41, Jan. 2004.
[3] Y. P. Zhang, "Wireless chip area network: A new paradigm for antennas, RF(MM)ICs, and communications," in *Proc. Asia-Pacific Microwave Conf.*, New Delhi, India, Dec. 15-18, 2004.
[4] M. Sun and Y. P. Zhang, "Performance of inter-chip RF-interconnect using CPW, capacitive coupler and UWB transceiver," *IEEE Trans. Microw. Theory Tech.*, vol. 53, no. 9, pp. 2650–2655, Sep. 2005.
[5] Y. J. Zheng, Y. P. Zhang, and Y. Tong, "A novel wireless interconnect technology using impulse radio for inter-chip communications," *IEEE Trans. Microw. Theory Tech.*, vol. 54, no. 4, pp. 1912–1920, Apr. 2006.
[6] Y. P. Zhang, Z. M. Chen, M. Sun, and J. He, "Wireless chip area networks: A new paradigm for RF microelectronics and radio communications," presented at the IEEE Workshop on Electrical Design of Advanced Packaging and Systems, Shanghai, China, Dec. 14–16, 2006.
[7] Z. M. Chen and Y. P. Zhang, "Inter-chip wireless communication channel: Measurement, characterization, and modeling," *IEEE Trans. Antennas Propag.*, vol. 55, no. 3, pp. 978–986, Mar. 2007.
[8] K. Kim, W. Bomstad, and K. K. O, "A plane wave model approach to understanding propagation in an intra-chip communication system," in *IEEE Int. Symp. AP-S*, Boston, 2001, vol. 2, pp. 166–169.
[9] K. Kim and K. K. O, "Characteristics of integrated dipole Antennas on bulk, SOI and SOS substrates for wireless communications," in *IEEE Proc. IITC*, San Francisco, 1998, pp. 21–23.
[10] A. B. M. H. Rashid, S. Watanabe, and T. Kikkawa, "Characteristics of integrated antenna on Si for on-chip wireless interconnect," *Jpn. J. Appl. Phys.*, vol. 42, pp. 2204–2209, Apr. 2003.
[11] S. Watanabe, A. B. M. H. Rashid, and T. Kikkawa, "Effect of high resistivity Si substrate on antenna transmission gain for on-chip wireless interconnects," *Jpn. J. Appl. Phys.*, vol. 43, pp. 2297–2301, Apr. 2004.
[12] Y. P. Zhang, M. Sun, and W. Fan, "Performance of integrated antennas on silicon substrates of high and low resistivities up to 110 GHz for wireless interconnects," *Microw. Opt. Tech. Lett.*, vol. 48, no. 2, pp. 302–305, Feb. 2006.
[13] Y. P. Zhang, L. H. Guo, and M. Sun, "High transmission gain inverted-F antenna on low-resistivity Si for wireless interconnect," *IEEE Electron Device Lett.*, vol. 27, no. 5, pp. 374–376, May 2006.
[14] K. T. Chan *et al.*, "Integrated antennas on Si with over 100 GHz performance, fabricated using an optimized proton implantation process," *IEEE Microw. Wireless Compon. Lett.*, vol. 13, no. 11, pp. 487–489, 2003.
[15] T. S. Rappaport, *Wireless Communications Principles and Practice*, 2nd ed. Upper Saddle River, NJ: Prentice Hall, Dec. 2002.
[16] X. L. Guo, R. Li, and K. K. O, "Design guidelines for reducing the impact of metal interference structures on the performance on-chip antennas," in *IEEE AP-S Int. Symp.*, Columbus, OH, Jun. 2003, vol. 1, pp. 606–609.
[17] N. G. Alexopoulos and I. E. Rana, "Mutual impedance computation between printed dipoles," *IEEE Trans. Antennas Propag.*, vol. AP-29, no. 1, pp. 106–111, Jan. 1981.
[18] D. M. Pozar, "Considerations for millimeter wave printed antennas," *IEEE Trans. Antennas Propag.*, vol. AP-31, no. 5, pp. 740–747, Sep. 1983.

Yue Ping Zhang received the B.E. and M.E. degrees from Taiyuan Polytechnic Institute and Shanxi Mining Institute of Taiyuan University of Technology, Shanxi, China, in 1982 and 1987, respectively, and the Ph.D. degree from the Chinese University of Hong Kong, Hong Kong, in 1995, all in electronic engineering.

From 1982 to 1984, he worked at Shanxi Electronic Industry Bureau, from 1990 to 1992, the University of Liverpool, Liverpool, U.K., and from 1996 to 1997, City University of Hong Kong. From 1987 to 1990, he taught at Shanxi Mining Institute and from 1997 to 1998, the University of Hong Kong. He was promoted to a Full Professor at Taiyuan University of Technology in 1996. He is now an Associate Professor and the Deputy Supervisor of Integrated Circuits and Systems Laboratories with the School of Electrical and Electronic Engineering, Nanyang Technological University, Singapore. He has broad interests in radio science and technology and published widely across seven IEEE societies. He has delivered scores of invited papers/keynote address at international scientific conferences. He has organized/chaired dozens of technical sessions of international symposia.

Dr. Zhang received the Sino-British Technical Collaboration Award in 1990 for his contribution to the advancement of subsurface radio science and technology. He received the Best Paper Award from the Second International Symposium on Communication Systems, Networks and Digital Signal Processing, held July 18–20, 2000, Bournemouth, U.K. and the Best Paper Prize from the Third IEEE International Workshop on Antenna Technology, held March 21–23, 2007, Cambridge, UK. He was awarded a William Mong Visiting Fellowship from the University of Hong Kong in 2005. He is listed in *Marquis Who's Who, Marquis Who's Who in Science and Engineering,* and *Outstanding Scientists of the 21st Century, Cambridge IBC 2000* . He serves on the Editorial Board of the *International Journal of RF and Microwave Computer-Aided Engineering* and was a Guest Editor of the Journal for the Special Issue "RF and Microwave Subsystem Modules for Wireless Communications." He also serves as an Associate Editor of the *International Journal of Microwave Science and Technology*. Furthermore, he serves on the Editorial Boards of IEEE TRANSACTIONS ON MICROWAVE THEORY AND TECHNIQUES and the IEEE MICROWAVE AND WIRELESS COMPONENTS LETTERS.

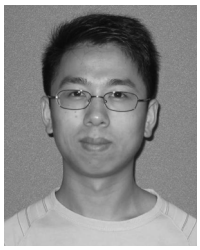

Zhi Ming Chen (S'04) was born in Jiangsu, China, in 1982. He received the B.Eng degree in electrical and electronic engineering from Nanyang Technological University, Singapore, in 2005, where he is currently working towards the Ph.D. degree in electrical and electronic engineering.

His research interests include study of inter-chip wireless interconnect system and RF transceiver design for wireless communication.

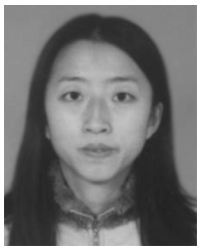

Mei Sun was born in Gansu, China, in 1980. She received the B.E. degree in electrical and information engineering from the Hunan University, China, in 2000, the M.E. degree in electronic engineering from Beijing Institute of Technology, China, in 2003, and the Ph.D. degree in electronic engineering from the Nanyang Technological University, Singapore, in 2007.

Since 2006, she has been a Research Associate with the Integrated Systems Research Laboratory, Nanyang Technological University, Singapore, where her research interests include intra- and inter-chip RF wireless communication system simulation and implementation, and integrated antenna design for wireless communication.

Dr. Sun received the Best Paper Prize from the Third IEEE International Workshop on Antenna Technology, March 21–23, 2007, Cambridge, U.K.